Available online at www.sciencedirect.com
SCIENCE DIRECT®
International Journal of Solids and Structures 43 (2006) 5593–5612
INTERNATIONAL JOURNAL OF SOLIDS and STRUCTURES
www.elsevier.com/locate/ijsolstr

A domain-independent integral for computation of stress intensity factors along three-dimensional crack fronts and edges by BEM

J.E. Ortiz *, V. Mantič, F. París

School of Engineering, Group of Elasticity and Strength of Materials, University of Seville, Camino de los Descubrimientos s/n, 41092 Seville, Spain

Received 4 May 2005
Available online 30 September 2005

Abstract

The present work deals with an evaluation of stress intensity factors (SIFs) along straight crack fronts and edges in three-dimensional isotropic elastic solids. A new numerical approach is developed for extraction, from a solution obtained by the boundary element method (BEM), of those SIFs, which are relevant for a failure assessment of mechanical components. In particular, the generalized SIFs associated to eigensolutions characterized by unbounded stresses at a neighbourhood of the crack front or a reentrant edge and also that associated to *T*-stress at the crack front can be extracted. The method introduced is based on a conservation integral, called *H*-integral, which leads to a new domain-independent integral represented by a scalar product of the SIF times some element shape function defined along the crack front or edge. For sufficiently small element lengths these weighted averages of SIFs give reasonable pointwise estimation of the SIFs. A proof of the domain integral independency, based on the bi-orthogonality of the classical two-dimensional eigensolutions associated to a corner problem, is presented. Numerical solutions of two three-dimensional problems, a crack problem and a reentrant edge problem, are presented, the accuracy and convergence of the new approach for SIF extraction being analysed.

Keywords: Stress intensity factors; Three-dimensional cracks; Edge singularities; Vertex singularities; Conservation integral; *H*-integral; Domain-independent integral; Boundary element method

1. Introduction

The evaluation of stress intensity factors (SIFs) associated to cracks has been a major task in linear elastic fracture mechanics since Williams (1957) and Irwin (1957) demonstrated that these parameters control the singular stress field near the crack tip. It has been shown experimentally that there is a critical value of SIF which

* Corresponding author. Fax: +34 954461637.
E-mail address: jortiz@esi.us.es (J.E. Ortiz).

0020-7683/$ - see front matter © 2005 Elsevier Ltd. All rights reserved.
doi:10.1016/j.ijsolstr.2005.08.003

controls fracture initiation. To assure the structural integrity of mechanical components in industry the SIF concept is widely used.

Analogous parameters which govern the singular stress field at the neighbourhood of an edge, corner in two-dimensions (Wieghardt, 1907; Williams, 1952), or a three-dimensional polyhedral vertex (Benthem, 1977; Bažant and Estenssoro, 1979), are usually also referred to as (generalized) SIFs. While the role of the SIF for cracks is well understood, the role of the SIFs for edges (corners in 2-D) in failure is under study currently. Most of the failure criteria at reentrant edges in brittle elastic materials are based on the SIF concept, see for example Seweryn (1994), Dunn et al. (2001) and Yosibash et al. (2004).

There are several numerical methods for SIFs calculation in the finite element and boundary element methods (FEM and BEM). Most of them could be classified in local or global methods, the former dealing with the local variables defined near the crack tip whereas the latter are based on the far field variables or variables associated to the whole domain.

The local methods, like the quarter-point singular element (Henshell and Shaw, 1975; Barsoum, 1976) and displacement and stress extrapolation methods (Chan et al., 1970), may be very sensitive, their accuracy being strongly dependent on the refinement near the crack front or edge in the discretized model.

The global methods are based, for example, on conservation integrals, like *J*-, *M*-, *L*- and *H*-integrals. Conservation integrals constitute a more robust approach since they eliminate the need to solve local singular stress fields very accurately. The *J*-integral method is an energy approach proposed originally for plane problems (Eshelby, 1956; Rice, 1968) and appears to be the first path-independent integral proposed to evaluate SIFs. To extract SIFs in mixed-mode cracks using *J*-integral, it is necessary to decouple the stress and strain fields into the symmetric mode I and both antisymmetric modes II and III, see Huber et al. (1993) and Rigby and Aliabadi (1993). The interaction integral or two-state conservation integral, based on the superposition of the two equilibrium states, was successfully used, for example, by Miyazaki et al. (1993) and Cisilino and Ortiz (2005), respectively, for 2-D and 3-D interface cracks using BEM. The *M*-integral is an attractive methodology formulated originally by Knowles and Sternberg (1978). Two-state conservation laws obtained from the *M*-integral (Chen and Shield, 1977) have recently been adapted to the evaluation of SIFs at 2-D corners and 3-D edges, respectively, by Im and Kim (2000) and Lee and Im (2003) using FEM. The two-state *L*-integral was employed by Choi and Earmme (1992) to compute SIFs for circular arc-shape cracks. The so-called *H*-integral is in fact the Bueckner (1973) work-conjugate integral, which is derived from the well-known 2nd Betti reciprocal theorem. It has been applied in several works for SIF calculation at 2-D corners in isotropic, anisotropic and dissimilar materials, see, for example, Sinclair et al. (1984), Carpenter (1984, 1995) and Szabó and Babuška (1991), for applications to homogeneous isotropic corners. For 3-D crack problems a path-independent expression was derived by Meda et al. (1998) starting from the *H*-integral. All of these methodologies based on path-independent integrals necessarily require the use of an auxiliary field. The fact that the *H*-integral computation requires only evaluation of natural variables like displacements and stresses represents an inherent advantage of this approach, which can imply its better accuracy in comparison with other conservation integrals that require gradients of displacements and/or stresses.

The BEM is ideally suited for the evaluation of conservation integrals. This is because the required displacements and stresses (and also their derivatives if required) at internal points can be obtained in BEM with a high accuracy from their boundary integral representations, as opposed to other numerical techniques, like FEM. For 3-D calculations, the conservation integrals are typically used in their so-called surface- or domain-independent form. When the surface-independent form of conservation integrals is adopted, the integration is performed along a contour in a plane perpendicular to the crack front and also over the surface enclosed by this contour, see, for example, Huber et al. (1993), Rigby and Aliabadi (1993) for *J*-integral applications and Meda et al. (1998) for *H*-integral applications. Li et al. (1985) and Shih et al. (1986) using FEM, and more recently Ortiz and Cisilino (2005) using BEM, showed that *J*-integral in its domain-independent expression is versatile, efficient and simple to implement numerically. To develop the domain-independent *J*-integral, an auxiliary function q, which can be interpreted as a virtual crack front advance, is incorporated, Li et al. (1985) and Shih et al. (1986).

The present work has been motivated by the need to develop a numerical tool to compute in a direct and precise way the SIFs along 3-D crack fronts and edges. For this purpose a new 3-D *H*-integral formulation will be developed starting from its 2-D formulation. The domain-independent representation for this integral is

presented together with the details of its BEM implementation. The present procedure allows directly all the SIFs which govern the singular elastic field in the eigenfunction expansion at an edge to be computed.

Two benchmark problems are studied in this work. The first one is a straight circular cylinder cracked to its centerline. The main feature of this problem, which has a known analytical solution, is the quadratic variation in the SIF K_I along the crack front. Thus, it represents an interesting and genuinely three-dimensional fracture problem. The proposed procedure has been applied to solve this problem, showing its accuracy and overall performance. A comparison with the FEM based approach by Meda et al. (1998) is presented. The second problem is a 3-D solid under tension, which includes a reentrant edge with the dihedral solid angle of 270°. A convergence study is presented and the effect of the free lateral surface on the boundary layer behaviour of the SIF along the edge is studied for various Poisson's ratios. Solving the above problems, it is found that the accurate values of the SIF are obtained by the present procedure without using very fine meshes or singular elements at the crack front and edge.

2. The three-dimensional linear elastic field near an edge

Consider a 3-D homogeneous linear elastic isotropic solid containing a straight edge with a constant dihedral solid angle ω (=2ϕ), see, for example, Fig. 1(a). Technically important is the case of a reentrant edge with $\omega > 180°$ and the particular case of a crack with $\omega = 360°$. Although the following analysis and the SIF extraction method introduced can be directly extended to any case of the classical homogeneous boundary conditions (free, fixed, symmetry or antisymmetry condition, etc.), for the sake of simplicity, only traction-free flat panels of the dihedral angle intersecting at the edge will be considered in what follows, which is typically the most important situation for technical applications.

Let (x,y,z) and (r,θ,z), respectively, be the Cartesian and the associated cylindrical coordinate system defined at the edge in the following way: z-axis coincides with the edge, x-axis and y-axis are perpendicular to the edge, x-axis being placed in the symmetry plane of the dihedral angle and y-axis being perpendicular to this plane.

Due to the isotropy of the material considered and the symmetry of the traction-free edge problem, an elastic solution at the neighbourhood of a straight edge can be decomposed into three modes called, extending the terminology of the classical fracture mechanics, the symmetric (opening) mode I and the two antisymmetric (shear and tear) modes II and III. The general expression of the asymptotic series expansion of the displacement field (neglecting rigid body motions) at the neighbourhood of an edge can be written in the form (Aksentian, 1967; Hartranft and Sih, 1969; Andersson et al., 1995):

$$\mathbf{u}(r,\theta,z) = \sum_{m=\mathrm{I,II,III}} \sum_{p\geqslant 1} \sum_{j\geqslant 0} K_{mpj}(z) r^{\lambda_{mp}+j} \mathbf{f}_{mpj}(\theta) \quad (\mathrm{Re}\lambda_{mp} \leqslant \mathrm{Re}\lambda_{mq},\ p<q) \tag{1}$$

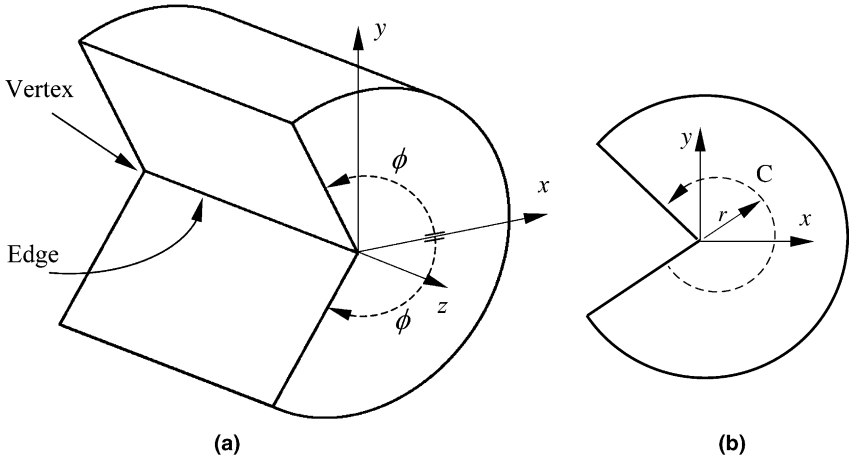

Fig. 1. (a) Example of a 3-D dihedral angle domain with a reentrant edge and two vertices. (b) Example of a 2-D corner.

where $\mathbf{u}$ is the displacement vector, index m denotes the above described modes, and index p denotes the order of an eigenmode associated to the corresponding 2-D corner problem.

The classical 2-D corner eigensolutions are represented in (1) by their singularity exponents λ_{mp} and their angular functions $\mathbf{f}_{mp0}$ denoted as $\mathbf{f}_{mp}$. The corresponding SIFs K_{mp0} are denoted as K_{mp}. The eigensolutions of the traction-free plane strain corner problem, corresponding to $m = \mathrm{I}$ and II, were comprehensively studied by Wieghardt (1907), Williams (1952) and Vasilopoulos (1988), the last work presenting tabulated singularity exponents, solutions of the transcendental characteristic equations:

$$\lambda_{\mathrm{I}p} \sin\omega = -\sin\lambda_{\mathrm{I}p}\omega \quad \text{and} \quad \lambda_{\mathrm{II}p} \sin\omega = \sin\lambda_{\mathrm{II}p}\omega \tag{2}$$

The traction-free antiplane corner problem, corresponding to $m = \mathrm{III}$, represents in fact the corner problem for the Laplace equation with homogeneous Neumann conditions, the characteristic equation being

$$\sin\lambda_{\mathrm{III}p}\omega = 0 \tag{3}$$

thus $\lambda_{\mathrm{III}p} = p\pi/\omega$. The condition of finite strain energy of the solution in the neighbourhood of the edge implies that the real part $\mathrm{Re}\,\lambda_{mp} > 0$ is required in (1). Adopting the following specially simple notation: $K_m = K_{m1}$, $\lambda_m = \lambda_{m1}$ and $\mathbf{f}_m = \mathbf{f}_{m1}$ for the most singular first terms ($p = 1$) associated to each mode $m = \mathrm{I}$, II and III, the classical fracture mechanics notation is recovered for these terms. Note that $1/2 < \lambda_{\mathrm{I}} < \lambda_{\mathrm{III}} < \lambda_{\mathrm{II}}$ for reentrant edges, except for a crack where $\lambda_m = 1/2$. Further details and references on 2-D corner eigensolutions can be found, for example, in Leguillon and Sanchez-Palencia (1987) and Szabó and Babuška (1991).

Indices $j \geqslant 1$ correspond to higher order additional terms (not present in a pure two-dimensional asymptotic expansion), sometimes called "shadow terms", originated by variation of the SIFs K_{mp} along the edge. In fact, K_{mpj} for $j \geqslant 1$ can be expressed as linear combinations of derivatives of K_{mp} (Hartranft and Sih, 1969; Andersson et al., 1995; Costabel et al., 2004).

Although in some exceptional cases (given by special configurations of boundary conditions, dihedral angle value and material properties), terms in form $r^{\lambda}(\log r)^q$, with q being a natural number, may appear in an elastic solution expansion at the edge, these cases will not be addressed in the present work.

The solutions of the characteristic equations in (2) and (3), with negative real part, denoted as λ_{mp} (for $p \leqslant -1$), also correspond to elastic solutions of the 2-D traction-free corner problems, in the sense that they fulfill the boundary conditions and the governing field equations. They have, however, unbounded displacements and unbounded energy at the corner tip, which is physically unrealistic, see Leguillon and Sanchez-Palencia (1987). Nevertheless, it is well known that these eigensolutions may be useful in the SIF extraction, this property being used in the present work as well.

It is useful, in particular for the purpose of comparison with other authors, to define the SIFs K_m in terms of stresses as:

$$K_m(z) = \lim_{r\to 0} c_m r^{1-\lambda_m} \sigma_m(r, \theta = 0, z) \tag{4}$$

where $\sigma_{\mathrm{I}} = \sigma_{\theta\theta}$, $\sigma_{\mathrm{II}} = \sigma_{r\theta}$ and $\sigma_{\mathrm{III}} = \sigma_{\theta z}$, and c_m is a normalization constant. In the present work the value $c_m = \sqrt{2\pi}$ is adopted according to the suggestion by Seweryn (1996). Note that the other possibility $c_m = (2\pi)^{1-\lambda_m}$ is also sometimes considered in the literature (Paegau et al., 1996) and that both definitions recover the classical SIF definition in the case of the crack with $\lambda_m = 1/2$.

3. The three-dimensional domain-independent integral

The path-independent integral for a 2-D crack called H-integral was originally developed by Bueckner (1973). To establish the path independency of this integral for a 2-D corner problem, the 2nd Betti's reciprocal theorem involving the actual elastic field and an appropriate auxiliary elastic field can be used. In the absence of volume forces and with traction-free corner faces in both, the actual and auxiliary, elastic fields, the H-integral is expressed as:

$$H = \int_C (T_i u'_i - T'_i u_i)\,\mathrm{d}C \tag{5}$$

where u_i and T_i (u'_i and T'_i) are displacement and traction vectors of the actual field (the auxiliary field), respectively, and C is an arbitrary path around the corner tip, see Fig. 1(b). Notice that $H = 0$ in (5) when both, actual and auxiliary, elastic solutions have a finite energy in the corner tip neighbourhood.

Consider, for simplicity, only real eigenvalues λ_{mp} hereinafter (see Leguillon and Sanchez-Palencia, 1987, for a similar analysis with complex eigenvalues). Elastic eigensolutions $r^{\lambda_{mp}}\mathbf{f}_{mp}(\theta)$ appearing in (1) are associated to the above 2-D corner problem. Then, a property of bi-orthogonality between the families of the eigenfunctions $\mathbf{f}_{mp}(\theta)$ associated to positive and negative eigenvalues λ_{mp}, respectively, can be shown (e.g., Leguillon and Sanchez-Palencia, 1987; Szabó and Babuška, 1991). This property means that H-integral in (5), taking the actual field given by an eigenfunction associated to λ_{mp} and the auxiliary field given by an eigenfunction associated to $-\lambda_{nq}$, is nonzero if and only if $m = n$ and $p = q$. Based on this orthogonality condition and using the field associated to the negative eigenvalue $-\lambda_{mp}$ as the auxiliary field, it is possible to show that (5) is proportional to the SIF K_{mp} in the actual field. Thus,

$$K_{mp} = \int_C (T_i u'_i - T'_i u_i)\,\mathrm{d}C \tag{6}$$

where an adequate normalization factor for the auxiliary field has been chosen.

A domain-independent integral for SIF computations along edges in 3-D problems can be deduced from (6) as will be shown in what follows. For this purpose, let us consider a straight edge represented in Fig. 2(a) as curved to better indicate the symmetry plane of the dihedral angle domain. Define a local coordinate system (x', y', z') with its origin at a global position z_n, where the SIF $K_{mp}(z_n)$ is evaluated, and with its axes x', y' and z' respectively parallel to the axes x, y and z. Let V define a dihedral angle cylindrical domain at the edge with the outer circular cylindrical surface of radius r_0 denoted as S_o. Let V_ε be another dihedral angle cylindrical domain of a small radius $\varepsilon > 0$, its outer circular cylindrical surface being denoted as S_ε. Let S be a closed boundary surface of the subtracted domain $V - V_\varepsilon$, formed by the following surfaces: S_ε (interior cylindrical surface of a radius ε), S_o (outer cylindrical surface), S_{-L} and S_{+L} (back and front plane base surfaces), S_1 and S_2 (dihedral angle plane faces) as shown in Fig. 2(b) and (c). Let a smooth continuous function $q(r, z')$ be defined in the domain V as the product $q(r, z') = q_r(r) \cdot q_z(z')$ (see Fig. 2(d) and (e)), where:

$$q_r(r) = \begin{cases} 1 \text{ for } r = 0 \\ 0 \text{ on } S_o \\ \text{otherwise smooth} \end{cases} \quad \text{and} \quad q_z(z') = \begin{cases} 0 \text{ on } S_{-L} \text{ and } S_{+L} \\ \text{otherwise smooth} \end{cases} \tag{7}$$

Let the dihedral angle faces be assumed traction-free for both, the actual and auxiliary, fields. Then, due to the fact that $q(r, z')$ vanishes on S_o, S_{-L} and S_{+L}, the following relation holds:

$$\int_{S_\varepsilon} \left[(T_i u'_i - T'_i u_i) q\right] \mathrm{d}S = \int_S \left[(T_i u'_i - T'_i u_i) q\right] \mathrm{d}S \tag{8}$$

Applying the divergence theorem to the right-hand side of (8), and taking into account that both fields satisfy the governing elasticity equations, assuming the same linear stress–strain relation for both fields, it is obtained that:

$$\int_{S_\varepsilon} \left[(T_i u'_i - T'_i u_i) q\right] \mathrm{d}S = \int_{V - V_\varepsilon} \left[\left(\sigma_{ij} u'_i - \sigma'_{ij} u_i\right) q_{,j}\right] \mathrm{d}V \tag{9}$$

Applying the Fubini theorem to the surface integral on the left-hand side of (9) the following relation is obtained:

$$\int_{-L}^{+L} \left[\int_{C_\varepsilon} (T_i u'_i - T'_i u_i)\,\mathrm{d}C\right] q_r(\varepsilon) q_z(z')\,\mathrm{d}z' = \int_{V - V_\varepsilon} \left[\left(\sigma_{ij} u'_i - \sigma'_{ij} u_i\right) q_{,j}\right] \mathrm{d}V \tag{10}$$

where C_ε is the circular contour of radius ε which lies in the x'–y' plane, Fig. 2(c).

According to the asymptotic series expansion of the actual elastic field in (1), this field can be decomposed, for a fixed value z', in (possibly singular) plane strain and antiplane terms and additional smooth terms. The additional terms are originated by the three-dimensional character of the actual field and the lowest possible

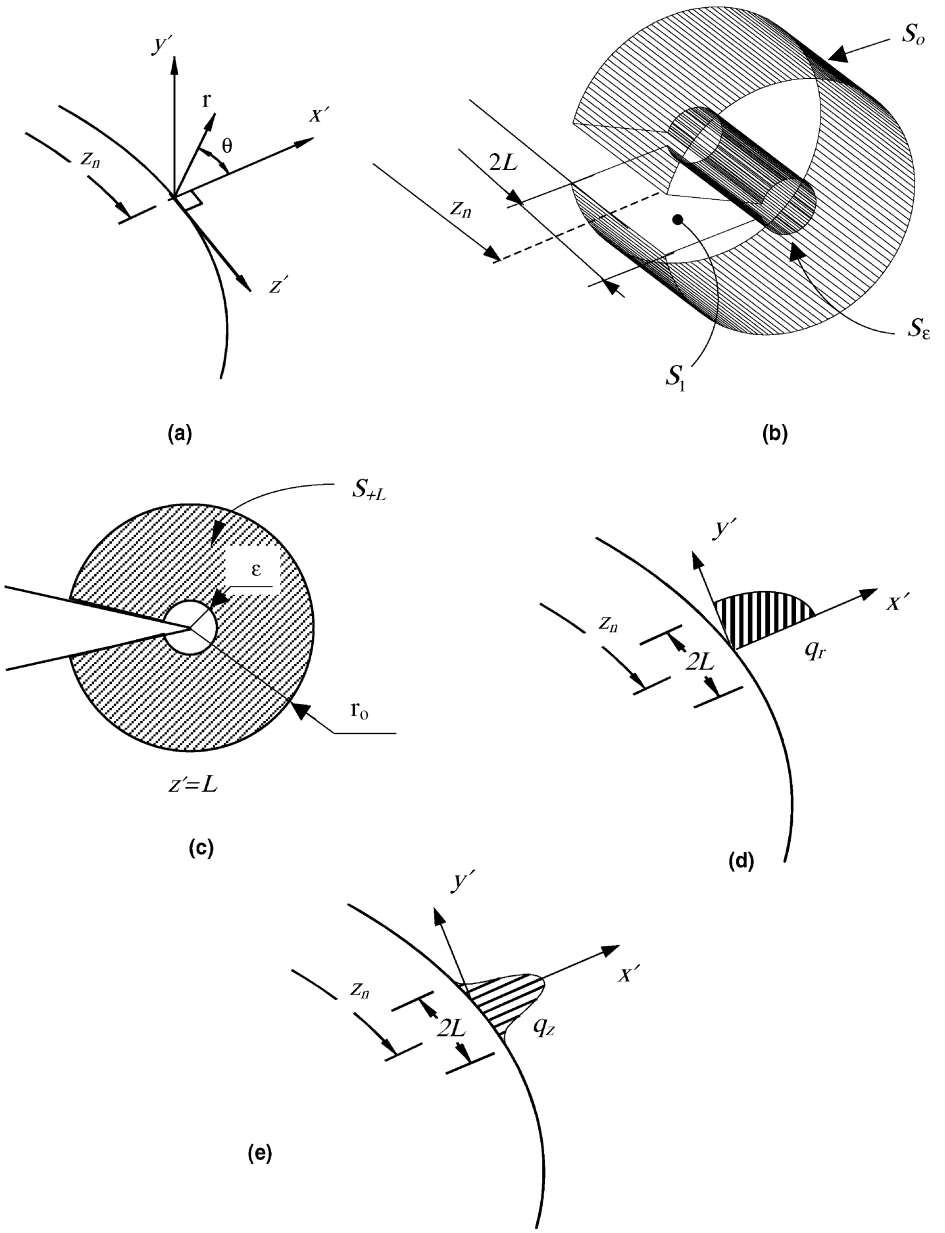

Fig. 2. (a) Definition of the local orthogonal Cartesian coordinates at point z_n placed along the edge. (b) Illustration of the surface S_ε and S_o. (c) Illustration of the surface S_{+L}. (d) The auxiliary function q_r along segment $2L$. (e) The auxiliary function q_z along segment $2L$.

order of these terms is $O(r^{\lambda_{sing.}+1})$, $\lambda_{sing.}$ representing the lowest singularity exponent λ_m appearing in the asymptotic series expansion of the elastic solution at the edge neighbourhood. In particular, in presence of the symmetric singular mode I, $\lambda_{sing.} = \lambda_I$. Thus, the integral over C_ε on the left-hand side in (10) can be decomposed into two integrals, the first one including only the plane strain and antiplane terms of the actual field, giving $K_{mp}(z')$ due to (6) and the fact that $\lim_{\varepsilon\to 0} q_r(\varepsilon) = 1$ from (7), and the second one including the additional smooth "shadow" terms. This second integral is in general of the order $O(\varepsilon^{\lambda_{sing.}+1-\lambda_{mp}})$. It vanishes in the limit $\varepsilon \to 0$ provided that the condition:

$$0 < \lambda_{mp} < \lambda_{sing.} + 1 \tag{11}$$

is verified. Therefore, as a consequence of the previously explained fact that the 2-D solution prevails near the corner tip, it is obtained under condition (11), that:

$$\int_{-L}^{+L} [K_{mp}(z') \cdot q_z(z')] \, \mathrm{d}z' = \int_V \left[\left(\sigma_{ij} u'_i - \sigma'_{ij} u_i \right) q_{,j} \right] \mathrm{d}V \tag{12}$$

As follows from Eq. (12), the integral on the right-hand side of (12) is a domain-independent integral, inasmuch as the left-hand side in (12) is independent of the domain V definition. Notice, however, that the definition of the function $q(r, z')$ depends on the radius of the outer surface S_o of the domain V.

Let us define the weighted average value of $K_{mp}(z')$ between $-L$ and $+L$ as:

$$\overline{K}_{mp}(z_n) = \frac{\int_{-L}^{+L} K_{mp}(z') q_z(z') \, \mathrm{d}z'}{\int_{-L}^{+L} q_z(z') \, \mathrm{d}z'} \tag{13}$$

Then using (12)

$$\overline{K}_{mp}(z_n) = \frac{\int_V \left[\left(\sigma_{ij} u'_i - \sigma'_{ij} u_i \right) q_{,j} \right] \mathrm{d}V}{\int_{-L}^{+L} q_z(z') \, \mathrm{d}z'} \tag{14}$$

$\overline{K}_{mp}(z_n)$ can be considered to be an approximation of $K_{mp}(z_n)$ for small lengths L. By partitioning the edge into a sufficient number of segments, $K_{mp}(z)$ can be approximated along this edge using values $\overline{K}_{mp}(z_n)$ obtained from (14) for a series of edge points z_n.

The components u'_i and σ'_{ij} in (14) are the displacements and stresses associated to the negative eigenvalue $-\lambda_{mp}$ of the 2-D corner problem. The adequate normalization factor of this auxiliary field is obtained from (14) taking eigensolutions u_i and σ_{ij} associated to the positive eigenvalue λ_{mp} and the constant unit SIF K_{mp}.

It should be pointed out that the condition (11) is actually not very restrictive from the practical point of view of technical applications, where crack and reentrant edge problems are of interest. In these cases the present procedure can be used to evaluate SIFs K_m (which are associated to unbounded stresses, with an exception for $m = \mathrm{II}$ where unbounded stresses appear only for dihedral angles $\omega > 257.45°$) and also SIF K_{I2}, in the crack case, associated to the term called T-stress.

4. BEM code implementation

The above explained procedure for computation of $\overline{K}_{mp}(z_n)$ has been implemented in a 3-D BEM code in the post-processing stage. The BEM code applied to solve 3-D isotropic elastic problems is based on the boundary element solution of the classical boundary integral equation (BIE) obtained from the Somigliana displacement identity, Chen and Zhou (1992). Considering, in general, mixed boundary conditions, the resulting BIE has a mixed character from the point of view of the Fredholm theory of linear integral operators, it being of the first or second kind, respectively, on the boundary part where displacements or tractions are prescribed. Assuming that rigid body motions have been removed by the displacements prescribed or by suitable point supports, the discretized BIE has a unique solution.

Some relevant characteristics of this code follow: isoparametric quadratic boundary element of nine nodes, numerical integration of regular integrals by Gaussian quadratures with 16 points using element subdivisions in the case of nearly singular integrals according to the widely used procedure developed by Lachat and Watson (1976), the rigid body motion approach for evaluation of the sum of the free term coefficients and the Cauchy principal value integrals. The resulting linear system is solved with Gaussian elimination. In order to asses the effect of the condition number of this system κ_2 (Golub and Van Loan, 1989) on the accuracy of the solution obtained, κ_2 has been evaluated for a sequence of refined meshes used in Section 6.2. An approximately linear dependence of κ_2 on the number of nodes has been observed, the relatively small value $\kappa_2 = 2.5 \times 10^4$ being obtained for the finest mesh of about 1500 nodes. This will allow an application of the present BEM code for SIF evaluation in more complicated bodies than those analysed in the present work.

As has been stated in Section 3, the computation of the domain integral of Eq. (14) for the SIF requires the stress and displacement fields u_i and σ_{ij} to be known within the integration volume V. The required values of

displacements and stresses at an internal point of the solid, $X \in \Omega$, are obtained from their boundary integral representations (BIRs):

$$u_i(X) = \int_\Gamma U^*_{ij} t_j \, d\Gamma - \int_\Gamma T^*_{ij} u_j \, d\Gamma \tag{15}$$

$$\sigma_{ij}(X) = \int_\Gamma D^*_{ijk} t_k \, d\Gamma - \int_\Gamma S^*_{ijk} u_k \, d\Gamma \tag{16}$$

where the kernels U^*_{ij} and T^*_{ij} are the fundamental displacement and traction solution, Γ is the boundary of the solid Ω, and the kernels D^*_{ijk} and S^*_{ijk} are deduced from U^*_{ij} and T^*_{ij} using differentiation and the constitutive stress–strain law. The above mentioned procedure of element subdivision is used in evaluation of the nearly singular integrals appearing in BIRs (15) and (16) at internal points $X \in \Omega$ close to the boundary.

The values of displacements and stresses at a boundary point $X \in \Gamma$ are directly evaluated from the BEM solution for boundary displacements and tractions using differentiation of displacement shape functions (e.g., Sládek and Sládek, 1986). At nodes situated at element junctions a simple averaging scheme is used to obtain a unique value of the stress tensor at these junctions.

5. Implementation of the domain integral evaluation

Computation of the SIF at a position z_n placed along the edge using the expression (14) requires the evaluation of a domain integral within a dihedral angle domain with a cylindrical outer surface that encloses an edge segment of the length $2L$. A natural choice in a BEM code is to consider z_n coincident with a node on the edge, while L is taken as the element side length or half-length (see Fig. 3). Notice that the use of a uniform mesh, assumed in the above analysis for simplicity of notation, is no restriction in the present procedure. The volume portion V of the solid Ω, in which the domain integrals are evaluated, is discretized using 27-node isoparametric (brick) volume cells, over which stresses and displacements are approximated by products of the cell interpolation functions Ψ_i and the nodal values of σ_{ij} and u_i. Nodal values of these variables are computed following the procedures described in Section 4, depending on whether the node is internal or lies on the solid boundary. Volume discretization is designed to have a web-style geometry around the edge, while the integration volumes are taken to coincide with the different rings of cells, see Figs. 5(a) and 6(c), respectively, for crack and edge problems studied in the next section. Gaussian quadrature with $8 \times 8 \times 8$ points is used to evaluate the domain integral in each volume cell.

As depicted in Fig. 3, three different cases need to be considered, depending on whether the node of interest M (corresponding to a position z_n) is situated in the middle of an element side (mid-side node), is shared by two elements (shared node), or is situated at the external surface (surface node). If the node M is a mid-side node or surface node, $2L$ (the segment of the edge over which the integral is computed) spans over one

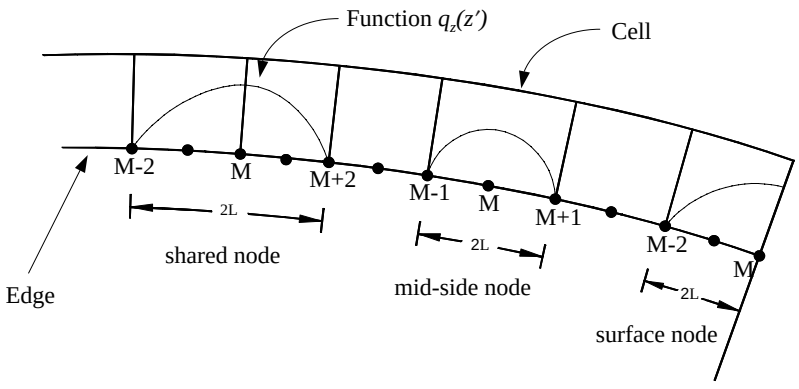

Fig. 3. Scheme of the volume cells in the edge region illustrating the function $q_z(z)$ for a shared node, a mid-node and a surface node.

element, connecting nodes $M-1$, M, and $M+1$ and nodes $M-2$, $M-1$ and M, respectively. On the other hand, if M is a shared node, $2L$ spans over two elements, connecting nodes from $M-2$ to $M+2$.

It has to be mentioned that the evaluation of $\overline{K}_{mp}(z_n)$ using (14) for a z_n-point coinciding with an end edge point (e.g. a surface node, see Fig. 3) is not allowed in general due to the necessity of verifying Eqs. (1) and (8) in the present procedure. Nevertheless, there are some particular cases where these equations are satisfied even for end edge points. For instance, it is allowed to evaluate $\overline{K}_{mp}(z_n)$ for $m = \mathrm{I}$, and II when the symmetry boundary conditions are prescribed at the surface perpendicular to the edge, and $\overline{K}_{\mathrm{III}p}(z_n)$ when the antisymmetry boundary conditions are prescribed at such a surface.

In this work both $q_z(z')$ and $q_r(r)$ are defined to vary quadratically in the directions tangential and normal to the edge, respectively. This bi-quadratic definition of q has been employed with excellent results in the computation of interaction integrals for cracks in previous works, see Cisilino and Ortiz (2005). Function $q = q_r(r)q_z(z')$ is interpolated at all points within the integration volume using the standard isoparametric volume elements:

$$q = \sum_{i=1}^{27} \Psi_i Q^i \tag{17}$$

where Ψ_i are the shape functions defined within each volume cell and Q^i are the nodal values of q function for the ith node. According to the definition of q (see Eq. (7)), $Q^i = 0$ if the ith node is on S_o, while for the rest of the nodes, Q^i are given by values of the product $q_r(r)q_z(z')$ at these nodes, in particular $Q^i = 1$ at the edge. Applying the chain rule:

$$q_{,j} = \sum_{i=1}^{27} \sum_{k=1}^{3} \frac{\partial \Psi_i}{\partial \zeta_k} \frac{\partial \zeta_k}{\partial x_j} Q^i \tag{18}$$

where ζ_k are the intrinsic coordinates in the cell isoparametric space.

6. Numerical examples

The numerical tool developed in this work is employed to test the numerical procedure proposed in the previous sections for the evaluation of SIFs $K_{mp}(z)$ (for m and p verifying condition (11)) along straight crack fronts and edges with traction-free faces in 3-D problems. In particular, the accuracy and convergence of this procedure is studied. Additionally, a parametric study of the influence of 3-D vertex singularity on the behaviour of the SIF along the edge is presented.

Two benchmark problems are studied in this work. The first one, with a known analytical solution, is a straight circular cylinder cracked to its centerline. A quadratic variation in $K_{\mathrm{I}}(z)$ along the crack front is considered, which makes it a genuinely 3-D fracture problem. The second problem is a solid with a reentrant edge of dihedral angle $\omega = 270°$ subjected to a tension load. This problem, which has been solved previously by other authors in the 2-D case, see Helsing and Jonsson (2002) for further references, is studied here in the 3-D case assuming traction-free lateral surfaces.

6.1. A three-dimensional crack

6.1.1. Problem description

Several three-dimensional crack problem solutions were proposed by Sinclair (1979), starting from Hartranft and Sih (1969) eigenfunction series expansions. Assuming a quadratic variation of $K_{\mathrm{I}}(z)$ along the straight crack front, Sinclair obtained a truncated series with only three terms. This problem will be solved in this section. The outer boundary of this problem can be arbitrary, but in order to compare with $K_{\mathrm{I}}(z)$ values obtained by Meda et al. (1998), using the surface-independent H-integral with FEM, a straight circular cylinder cracked to its centerline with the length of the cylinder l equal to unity (coincident with the crack width) in the z-direction and a radius a (coincident with the crack length) has been chosen in the present work. The cylindrical domain problem is described in cylindrical coordinates (r, θ, z) with the origin O placed at one

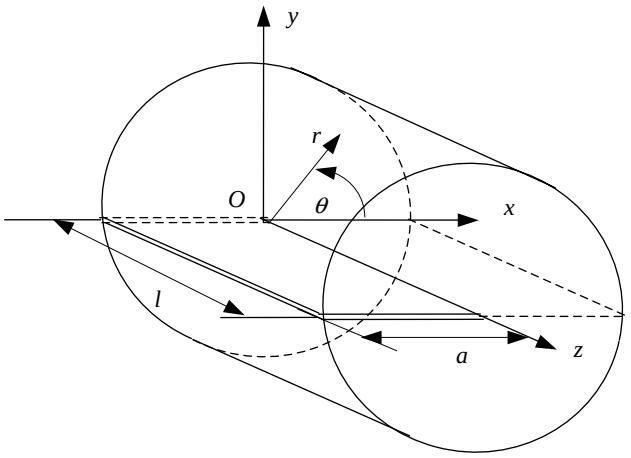

Fig. 4. Three-dimensional crack geometry.

extreme of the crack front, see Fig. 4. The complete expressions of the displacement and stress solutions of the problem by Meda et al. (1998) have been rewritten to a suitable form and are given in Appendix A.

The SIF for this problem can be identified using the expression for $\sigma_{\theta\theta}$ in Eq. (A.2) and following the definition given in (4):

$$K_{\mathrm{I}}(z) = 36\sqrt{2\pi}k \cdot z^2 \tag{19}$$

It is worth noting that the expression of displacements in Eq. (A.1) has the same structure as the expression in (1) for displacements at the neighbourhood of a general 3-D edge. The terms in Eq. (A.1) of the order $\mathrm{O}(r^{\lambda_{\mathrm{I}}})$, $\lambda_{\mathrm{I}} = \lambda_{\mathrm{II}} = 1/2$, affected by the function $K_{\mathrm{I}}(z)$ represent the classical plane strain behaviour when $r \to 0$, as was commented in Section 2. The terms in Eq. (A.1) of the order $\mathrm{O}(r^{\lambda_{\mathrm{I}}+j})$, $j = 1$ and 2, represent additional smoother "shadow" terms. Correspondingly, the terms in Eq. (A.2) of the order $\mathrm{O}(r^{\lambda_{\mathrm{I}}-1})$ represent the plane strain behaviour when $r \to 0$, and the terms of the order $\mathrm{O}(r^{\lambda_{\mathrm{I}}+j-1})$ represent additional smoother terms.

6.1.2. BEM model

In 3-D crack or reentrant edge problems it is crucial to consider some characteristic features of the solution in the design of the numerical BEM model in order to achieve a reasonable accuracy using an acceptable computing time on a computer with a modest performance. Specifically a refinement is usually required in the direction towards the crack front and along the crack front in the direction towards the vertices, where a strong variation of SIFs can be expected.

In this sense and in order to achieve a relatively high density of elements near the crack front keeping reduced size of the BEM model and computational costs, a small radius of the cylindrical domain, $a = 0.2l$, has been chosen and the symmetry of the problem with respect to the plane $y = 0$ has been used in the present study. Thus, the model applied is confined only to the region $y > 0$. Some details of the BEM mesh are given in what follows. The meshes on the back ($z = 0$) and front ($z = 1$) surfaces are subdivided in the radial direction into four radial regions: two elements of size 0.0035 being placed in the first region just at the crack front, three elements of size 0.007 in the second region, three elements of size 0.028 in the third region, and one element of size 0.088 being placed in the fourth periphery region. In the circumferential direction and with the exception of the elements adjacent to the crack front the mesh is divided into eight equally sized elements. On the other two surfaces (curved cylindrical surface and the surface given by $y = 0$) the mesh is divided into six elements of equal length in the z-direction, and in accordance with the back and front surface discretization in the circumferential direction. Fig. 5(a) illustrates the strategy applied for the BEM model design. This mesh has 284 quadratic elements with 1138 nodes, it being a reasonable mesh for the present problem in accordance with the experience of the authors.

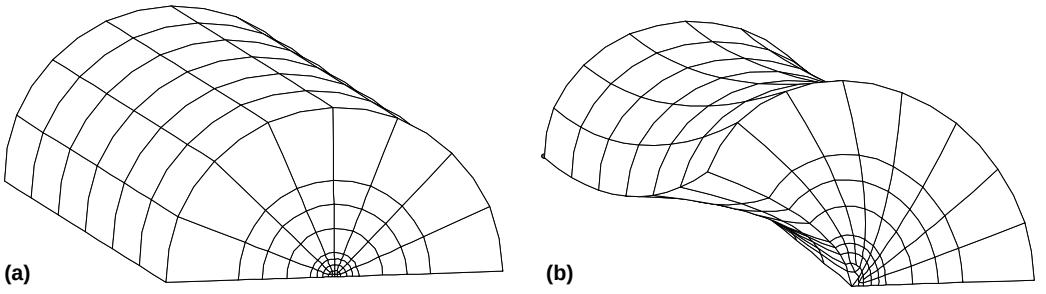

Fig. 5. (a) Schematic representation of BEM mesh. (b) Mode l deformed.

Boundary conditions for the problem are prescribed using expressions of displacements and stresses given in Eqs. (A.1) and (A.2). Thus, the symmetry boundary condition, $\bar{u}_z = \bar{\sigma}_{rz} = \bar{\sigma}_{\theta z} = 0$, is imposed on the back surface ($z = 0$, $0 < r < 0.2$, $0 < \theta < \pi$); a mixed boundary condition is prescribed in terms of $\bar{u}_z, \bar{\sigma}_{rz}$ and $\bar{\sigma}_{\theta z}$ on the front surface ($z = 1$, $0 < r < 0.2$, $0 < \theta < \pi$); the traction-free conditions, $\bar{\sigma}_{\theta\theta} = \bar{\sigma}_{r\theta} = \bar{\sigma}_{\theta z} = 0$, are prescribed on the crack face ($\theta = \pi$, $0 < r < 0.2$, $0 < z < 1$); the symmetry boundary condition, $\bar{u}_\theta = \bar{\sigma}_{r\theta} = \bar{\sigma}_{\theta z} = 0$, is imposed ahead of the crack ($\theta = 0$, $0 < r < 0.2$, $0 < z < 1$); traction conditions in terms of $\bar{\sigma}_{rr}$, $\bar{\sigma}_{r\theta}$ and $\bar{\sigma}_{rz}$ are prescribed along the curved surface ($r = 0.2$, $0 < z < 1$, $0 < \theta < \pi$). In order to remove a rigid body translation in the x-direction, displacement u_x is prescribed at the point $r = 0.2$, $\theta = 0$ and $z = 0$, which corresponds to a corner point of the domain. It has been preferred to avoid fixing a point of the crack front in order to avoid possible local perturbations originated by this support condition there.

SIF $\overline{K}_{\mathrm{I}}(z)$ is computed using the integral in (14) for a semi-cylinder domain of integration with one cell in the z-direction corresponding to a boundary element along the crack front. $\overline{K}_{\mathrm{I}}(z)$ is computed for the positions coincident with the nodes situated at the crack front as was explained in Section 5. In order to test the independency of the domain in the integral in (14), $\overline{K}_{\mathrm{I}}(z)$ is calculated using three cylinders with radii $r/a = 0.07$, 0.105 and 0.14, having 16, 24 and 32 cells, respectively. The total number of cells defined in this model is 192.

6.1.3. Results and discussion

Values of $\overline{K}_{\mathrm{I}}(z)$ for the three cylinders at each node along the crack front using the present BEM approach are shown in Table 1. These values are normalized by the exact value of K_{I} at $z = 1$ from (19). It can be observed that the values of $\overline{K}_{\mathrm{I}}(z)$ obtained are approximately independent of the domain integration for all the nodes. The percentage of the normalized error, $\%E(z)$, achieved in the integration cylinder with the greatest radio, is also shown in Table 1, where the normalized error $E(z)$ is defined as:

$$E(z) = \frac{[\overline{K}_{\mathrm{I}}(z) - K_{\mathrm{I}}(z)]}{\max_{(0 \leqslant z \leqslant 1)} |K_{\mathrm{I}}(z)|} \tag{20}$$

Table 1
Normalized values $\overline{K}_{\mathrm{I}}(z)/K_{\mathrm{I}}(z=1)$ for the cylinder crack problem, using the present BEM model and FEM model by Meda et al. (1998)

z	$\overline{K}_{\mathrm{I}}(z)/K_{\mathrm{I}}(z=1)$			$\%E(z)$ ($r/a = 0.14$)	$\%E(z)$ (Meda et al., 1998)
	r/a 0.07	0.105	0.14		
0.000	0.01987	0.01797	0.01681	1.681	
0.083	0.02738	0.02527	0.02410	1.721	
0.167	0.05117	0.04871	0.04733	1.944	
0.250	0.07533	0.07315	0.07182	0.932	1.000
0.333	0.12119	0.12005	0.11927	0.838	
0.417	0.17409	0.17392	0.17363	−0.026	
0.500	0.25124	0.25162	0.25164	0.164	0.500
0.583	0.33509	0.33608	0.33633	−0.356	
0.667	0.44261	0.44378	0.44411	−0.077	
0.750	0.55824	0.55974	0.56011	−0.238	3.749
0.833	0.69830	0.70065	0.70178	0.790	
0.917	0.84262	0.84668	0.84872	0.784	

Meda et al. (1998) applied a surface-independent H-integral formulation in the FEM to obtain $K_I(z)$ for the same problem. Their FEM mesh consists of 408 quadratic brick elements with 1401 nodes, the square-root singularity along the crack front being captured by using quarter-point elements. Results obtained by Meda et al. (1998) are also shown in Table 1. Comparing both conservation integral methods and BEM and FEM models, it can be seen that results for $\overline{K}_I(z)$ obtained in the present work present a better accuracy.

In general, an excellent agreement is found between the analytical and computed results, the percentage of the normalized error increasing slightly when the evaluation point approaches the back and front surfaces. Apparently, the proximity of the back and front surfaces has a negative influence on the accuracy of the BEM results in the interior points, which could make sensitive the computation of $\overline{K}_I(z)$ by (14). If this is so, then it would be possible to calculate $\overline{K}_I(z)$ with a higher precision, improving, on one hand, the accuracy of both the displacement and stress values used in the domain integral in (14), and, on the other hand, the accuracy of the numerical integration method applied.

To see this effect, the same procedure is repeated to obtain values of $\overline{K}_I(z)$ but now using the analytical values of the displacement and stress values calculated from Eqs. (A.1) and (A.2), respectively, at the Gaussian points of volume cells. Additionally, values of $\overline{K}_I(z)$ are obtained via an analytical integration of (14) using analytical expressions for displacements and stresses. For this purpose formula (14) has been implemented in Mathematica (Wolfram, 1991).

The results are shown for $r/a = 0.14$ in Table 2, label (I) is used for the results using BEM model, label (II) for the numerical integration with analytical displacements and stresses at Gaussian points in volume cells, and label (III) for a completely analytical evaluation of (14). The percentage of the normalized error with respect to the analytic values of $K_I(z)$ for these three cases is also shown in the same table. From these values, it can be seen that error is, for example at $z = 0$, 1.681%, 0.556% and 4.73E−04%, respectively, for the above cases (I), (II) and (III). This fact proves that there is an important source of error in using the BEM results in volume cell nodes and in a subsequent interpolation of these nodal values to the cell Gausssian points, but also that there is still a not negligible source of error in applying a numerical integration with $8 \times 8 \times 8$ Gaussian points in each volume cell. Notice that an error, although very small, appears when an analytical integration is used in (14), due to the fact that $\overline{K}_I(z)$ is an average value of $K_I(z)$ along a crack front segment weighted by a $q_z(z)$ function. The very small value of the error achieved in the analytical evaluation of (14) means that the error associated to the averaging procedure along the crack front segment is very small, at least in the case of a smooth behaviour of $K_I(z)$ as in the present problem.

The present procedure to evaluate SIFs is not only valid for small integration volume since the integral in (14) is a domain-independent integral. To check this feature $\overline{K}_I(z)$ is calculated for cylinders of radii equal to $0.5/l$, $1.0/l$, $2.5/l$ and $5.0/l$ with 8, 16, 24 and 32 cells, respectively, using the analytic values of displacements and stresses in the Gaussian points of volume cells. The results for $\overline{K}_I(z)$, normalized by $K_I(z = 1)$, are shown

Table 2
$\overline{K}_I(z)$ values normalized with respect to $K_I(z = 1)$ for the crack problem for radius of the cylindrical integration domain $r/a = 0.14$

z	$\overline{K}_I(z)/K_I(z = 1)$			%$E(z)$ (I)	%$E(z)$ (II)	%$E(z)$ (III)
	Using BEM (I)	Numerical integration (II)	Analytic integration (III)			
0.000	0.01681	0.00556	4.73E−07	1.681	0.556	4.73E−05
0.083	0.02410	0.00833	0.00689	1.721	0.144	7.95E−04
0.167	0.04733	0.03333	0.02789	1.944	0.544	2.61E−04
0.250	0.07182	0.06389	0.06250	0.932	0.139	6.65E−04
0.333	0.11927	0.11667	0.11089	0.838	0.578	1.58E−04
0.417	0.17363	0.17500	0.17389	−0.026	0.111	1.93E−04
0.500	0.25164	0.25555	0.25000	0.164	0.555	2.22E−04
0.583	0.33633	0.34167	0.33989	−0.356	0.178	3.68E−04
0.667	0.44411	0.45000	0.44489	−0.077	0.511	4.26E−04
0.750	0.56011	0.56389	0.56250	−0.238	0.140	6.09E−04
0.833	0.70178	0.70003	0.69389	0.790	0.614	8.00E−04
0.917	0.84872	0.84167	0.84089	0.784	0.079	8.81E−04

Application of BEM results, numerical integration and analytic integration in (14).

Table 3
Values of $\overline{K}_I(z)$ normalized by $K_I(z=1)$ for the crack problem

z	$\overline{K}_I(z)/K_I(z=1)$					$\%E(z)$ $r/l=5$
	r/l	0.5	1.0	2.5	5.0	
0.000		0.00555	0.00555	0.00563	0.00528	0.528
0.083		0.00833	0.00833	0.00840	0.00805	0.117
0.167		0.02500	0.02500	0.02505	0.02488	0.517
0.250		0.06388	0.06390	0.06398	0.06360	0.113
0.333		0.10835	0.10835	0.10843	0.10823	0.553
0.417		0.17500	0.17500	0.17508	0.17473	0.088
0.500		0.24718	0.24720	0.24733	0.24710	0.533
0.583		0.34165	0.34168	0.34175	0.34138	0.158
0.667		0.44165	0.44168	0.44188	0.44160	0.493
0.750		0.56388	0.56390	0.56398	0.56360	0.124
0.833		0.69173	0.69175	0.69203	0.69173	0.602
0.917		0.84165	0.84168	0.84175	0.84138	0.069

Application of analytic values for displacements and stresses in Gaussian points of volume cells and numerical integration.

in Table 3. The percentage of normalized error of $\overline{K}_I(z)$ computed using the cylinder with the largest ratio is also shown in Table 3. All the values obtained are in concordance with the results for $r/a = 0.14$ presented formerly in Table 2.

6.2. A reentrant edge

6.2.1. Problem description

The second example consists of a thick panel with a V-notch of angle $2\alpha = 90°$, corresponding to a dihedral solid angle $\omega = 270°$, and subjected to a uniaxial remote tension $\bar{\sigma}$. The mechanical properties are: Young elastic modulus $E = 210$ GPa and Poisson's ratio $v = 0.3$.

The singularity exponents of an elastic field at the neighbourhood of the above reentrant edge are given by the singularity exponents of the corresponding traction-free 2-D corner subjected to a plane strain state, the principal singularity exponent being $\lambda_I = 0.54448$ (Vasilopoulos, 1988), which has associated symmetrical fields in stresses and displacements, see Section 2.

6.2.2. BEM model

The model dimensions and boundary conditions are shown in Fig. 6 together with a view of the BEM mesh, which takes advantage of the two symmetry planes of the problem (at $y = 0$ and $z = 0$). The BEM mesh consists of 112 quadratic elements and 467 nodes. Five elements are placed along the reentrant edge of length t, and 30 elements are used on the bottom surface. The element dimensions in this face are graded towards the free front-surface, the smallest one being equal to $t/7$. Four rings of cells with radii r/w equal to 0.1, 0.2, 0.3 and 0.4 are placed around the edge for SIF $K_I(z)$ computations, 80 volume cells being employed for this purpose.

6.2.3. Results and discussion

In order to verify the accuracy of the present procedure when applied to a reentrant edge problem, the corresponding plane strain problem, for which numerical results of a high accuracy have been published by Helsing and Jonsson (2002), is studied first, reproducing the plane strain solution in a 3-D BEM model. The percentages of the difference between the computed values for K_I in the present work and those obtained by Helsing and Jonsson (2002), normalized by the accurate value of K_I, are presented in Table 4, for three points of the edge, on both the front and back surfaces and on the mid-plane of the specimen. For each edge point, K_I is computed using three cylindrical integration domains. As can be seen, the results show only a very slight variation for different domain integrations and very good agreement with the published accurate solution. The relative differences between both solutions are always less than 1%. The improvement in $\%E$ with increasing values of r/w is consistent with the fact that the BEM solution far from the edge is less polluted

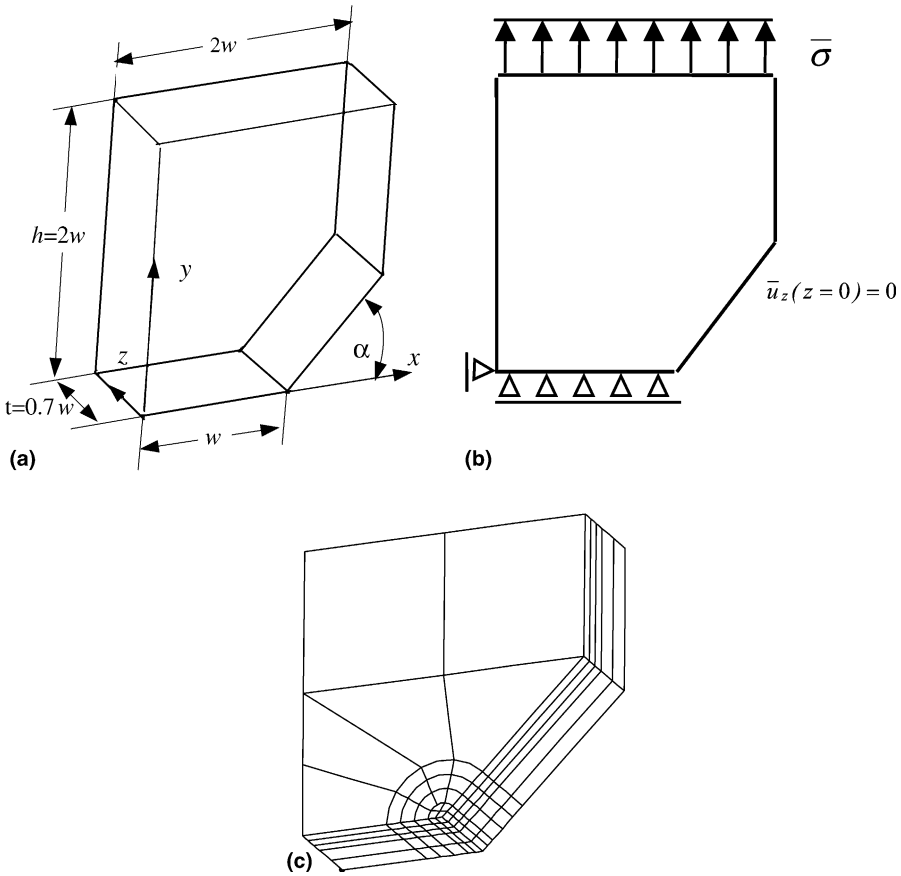

Fig. 6. Three-dimensional corner: (a) problem geometry, (b) boundary conditions, and (c) schematic representation of BEM mesh.

Table 4
Percentage of the relative differences (%E) of $\overline{K}_{\mathrm{I}}$ values in plane strain state with respect to the solution by Helsing and Jonsson (2002)

z/t	%$E(z/t)$		
	r/w	0.2	0.3	0.4
0.000		0.933	0.867	0.821
0.500		0.958	0.861	0.782
1.000		0.999	0.853	0.746

by an edge singularity, although this improvement is not too noticeable, which supports the notion that the use of coarse meshes yields good accuracy.

Results for $\overline{K}_{\mathrm{I}}(z)$ in the genuine 3-D reentrant edge problem are shown in Table 5, and $\overline{K}_{\mathrm{I}}(z)$ values obtained using the cylindrical integration domain with the largest radius are plotted in Fig. 7, both results being normalized by K_{I}-value of the plane strain problem. It can be observed in Table 5 that the values of $\overline{K}_{\mathrm{I}}(z)$ for edge points are approximately independent of the size of the integration domain. It is seen from Fig. 7 that the values of $\overline{K}_{\mathrm{I}}(z)$ decrease towards the free surface at $z = t$. Due to the fact that the rate of this decrease for points near the free surface is very high, two additional more refined models have been developed with the purpose of capturing the rapid changes in $K_{\mathrm{I}}(z)$ and verifying the convergence of the present procedure. The second BEM mesh has 10 elements placed along the reentrant edge, the element lengths along the edge being one half of the element lengths of the first BEM mesh. A similar strategy has been used for the third mesh, so it has 20 elements along the edge. These meshes will be referred to as A, B and C, respectively. Thus, mesh B has 202 quadratic elements with 827 nodes and mesh C has 382 quadratic elements with 1547 nodes.

Table 5
$K_I(z)$ values normalized by K_I in plane strain for the 3-D edge problem

z/t	$\overline{K}_I(z)/K_I$				
	r/w	0.1	0.2	0.3	0.4
0.0000		1.040208	1.043241	1.043923	1.044147
0.1430		1.039802	1.042853	1.043555	1.043793
0.2860		1.035835	1.038951	1.039644	1.039868
0.4290		1.030563	1.033805	1.034534	1.034752
0.5710		1.023396	1.026698	1.027454	1.027726
0.6430		1.011332	1.014786	1.015523	1.015741
0.7140		0.997644	1.001162	1.001932	1.002201
0.7860		0.981637	0.985268	0.985932	0.986137
0.8570		0.942022	0.945624	0.946572	0.947041
0.9290		0.885028	0.887359	0.888443	0.889335

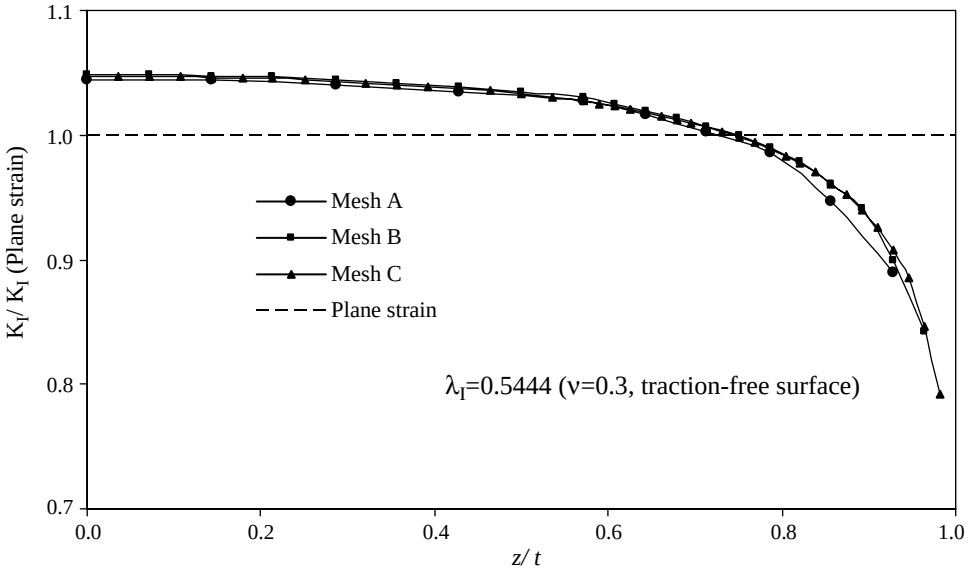

Fig. 7. $\overline{K}_I(z)$ values for the 3-D edge problem normalized by K_I in plane strain.

For $\overline{K}_I(z)$ computations, 160 and 320 cells are employed, respectively, in B and C mesh. The values of $\overline{K}_I(z)$ obtained by meshes B and C are also plotted in Fig. 7. Values of $\overline{K}_I(z)$ obtained by these two meshes (B and C) are practically coincident along a large part of the edge, the values obtained then being considered reliable enough and of a sufficient accuracy. However, for points near the free surface there are some slight variations between results by these two meshes. Thus a more refined mesh might be required in order to obtain results of a high accuracy in this zone. From results of mesh C there is some clear evidence that $K_I(z)$ vanishes for $z/t \to 1$, this behaviour being studied in what follows.

The value of $\overline{K}_I(z)$ for $z/t = 1$ has not been presented in Table 5 and Fig. 7, because the present domain-independent integral method is not strictly applicable at the intersection of the edge with a free surface. Additionally, the elastic solution at this vertex point has a purely 3-D nature, the intersection of the edge and the free surface proving to have a different singularity order than λ_m in plane strain, and as will be seen it may be weaker or stronger. In general, the 3-D vertex singularity exponent λ_{3D} depends on the boundary conditions at the edge faces and the exterior surface, Poisson's ratio v, the intersection angle of the edge with the surface and the symmetry of the solution (symmetric or antisymmetric modes), see Leguillon (1995). In Table 6, we reproduce singularity exponent λ_{3D} for a crack (included here for comparison) and a reentrant edge ($2\alpha = \pi/2$) both

Table 6
3-D vertex singularity exponent λ_{3D} for the crack and edge ($2\alpha = \pi/2$) that intersect perpendicularly a free surface

ν	$2\alpha = 0°$		$2\alpha = \pi/2$	
	λ_{3D}-symmetric	λ_{3D}-antisymmetric	λ_{3D}-symmetric	λ_{3D}-antisymmetric
0.00	0.50	0.50	0.544	0.908
0.15	0.515	0.44	0.576	0.837
0.30	0.55	0.40	0.623	0.787
0.49			~0.700	

intersecting perpendicularly a free surface. The values for the crack have been taken from Leguillon (1995) and for the edge from Savruk and Shakarayev (2001).

For both crack and edge λ_{3D} increases with ν for symmetric mode ($m = \mathrm{I}$) and decreases for plane antisymmetric mode ($m = \mathrm{II}$), note that λ_{3D} coincides with λ_m when $\nu = 0$. The singularity exponent λ_{3D} at the end of the edge may affect the SIFs behaviour along the edge associated to the singularity exponents λ_m, see Leguillon and Sanchez-Palencia (1999). In order to investigate the influence of the change of the vertex singularity over the classical SIF, the 3-D corner presented in Fig. 6 is studied using mesh C with ν equal to 0.0, 0.15, 0.3 and 0.49, the curves of $\overline{K}_{\mathrm{I}}(z)$ being shown in Fig. 8. When Poisson's ratio $\nu = 0$ ($\lambda_{\mathrm{I}} = \lambda_{3D}$), the governing equations decouple and the originally 3-D problem reduces in fact to that of the plane strain case, with the result that $K_{\mathrm{I}}(z)$ remains constant along the edge, its value being equal to the K_{I} value in the plane strain case. For all the other cases, it can be observed that values of $\overline{K}_{\mathrm{I}}(z)$ increase with increasing ν for small values of z/t with respect to the plane strain values of K_{I}, and decrease very rapidly for edge points near to the free surface, exhibiting some kind of asymptotic behaviour.

For similar problems in cracks such an asymptoptic behaviour was studied by Nakamura and Parks (1988), Leguillon and Sanchez-Palencia (1999) and Kwon and Sun (2000).

Following the approach by Leguillon and Sanchez-Palencia (1999) a simple analysis of the asymptotic behaviour for K_m at the neighbourhood of the 3-D corner will be presented. Let us estimate the asymptotic behaviour of the SIF $K_m(z_c)$ near the 3-D corner singularity, z_c denoting the distance to a reference point O', placed at the edge, from the 3-D vertex referred to as point O. Let a point P be situated at a distance R from O and a distance r from O', Fig. 9, distances z_c, R and r being related by relations $z_c = R\cos\varphi$ and $r = R\sin\varphi$. Let the displacement field at the point P be approximated in the following two ways,

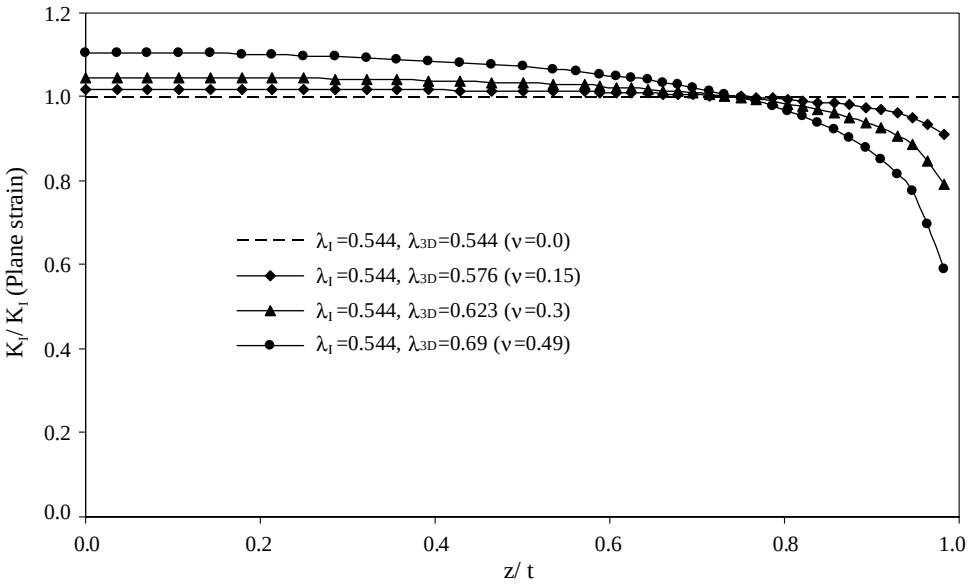

Fig. 8. $\overline{K}_{\mathrm{I}}(z)$ values for 3-D edge normalized by K_{I} in plane strain, for different values of Poisson's ratio ν.

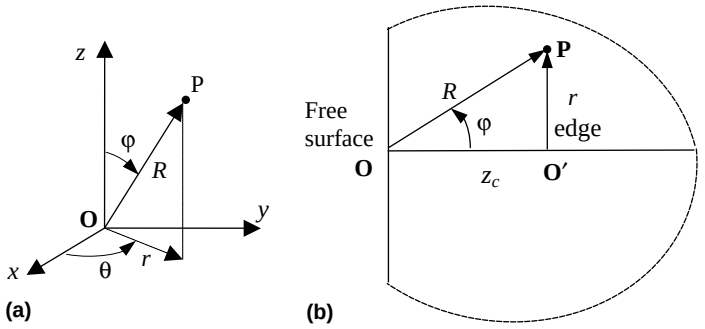

Fig. 9. (a) Spherical coordinates. (b) The end point of an edge at a free surface.

$\mathbf{u} \cong K_{3D} R^{\lambda_{3D}} \mathbf{f}_{3D}(\theta, \varphi)$ and $\mathbf{u} \cong K_m(z_c) r^{\lambda_m} \mathbf{f}_m(\theta)$. The first expression represents a 3-D vertex singularity behaviour and is referred to the point O (K_{3D} is the SIF associated to the vertex), whereas the second expression represents a 2-D singularity behaviour and is referred to the point O'. Changing the variables, expressing r and R in terms of z_c and an angle φ, and comparing both expressions of displacements, it yields, at the leading order, $K_m(z_c) \approx K_{3D} z_c^{\lambda_{3D} - \lambda_m}$, which determines the asymptotic behaviour for $K_m(z_c)$ when $z_c \to 0$, see Leguillon and Sanchez-Palencia (1999). If $\lambda_{3D} > \lambda_m$ the SIF $K_m(z_c)$ tends to zero and if $\lambda_{3D} < \lambda_m$ the SIF $K_m(z_c)$ tends to infinity. When the external surface is traction-free, these behaviours of $K_m(z_c)$ are respectively associated to a symmetric mode ($m = \mathrm{I}$), and an antisymmetric mode ($m = \mathrm{II}$).

In Fig. 10 $K_{\mathrm{I}}(z_c)$ obtained for three different values of the Poisson ratio v are plotted in log–log scale in the range of z/t between 0.75 and 0.95. There are marked tendencies of the $K_{\mathrm{I}}(z_c)$ values presented to follow straight lines, which corresponds to the above explained power asymptotic behaviour. The values for λ_{3D} obtained applying a linear regression to the log–log scale plots are 0.5768, 0.6217 and 0.7093 for v equal to 0.15, 0.30 and 0.49, respectively. The percentages of the relative difference of these values and the values showed in Table 6 are 0.14%, −0.21% and 1.33%, respectively, which can be considered as excellent results taking into account that a simple not specialized procedure has been used for 3-D singularity exponent evaluation. These errors are due to the lack of a stronger mesh refinement in the thickness direction in the zone close to the free

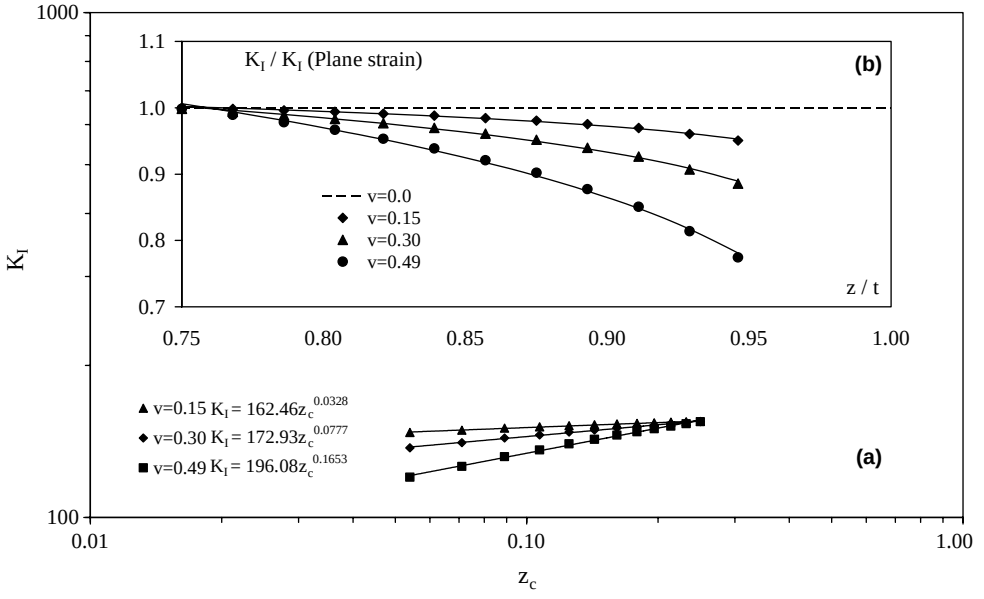

Fig. 10. (a) $K_{\mathrm{I}}(z_c)$ values vs. z_c coordinate in log–log scale in the range of z/t between 0.75 and 0.95. (b) $K_{\mathrm{I}}(z)$ values vs. z/t together with the asymptotic curves obtained.

surface in the present BEM model. In Fig. 10, $K_I(z)$ values are also plotted in standard linear scale together with the approximated asymptotic curves obtained.

7. Conclusions

A domain-independent integral formulation for the numerical computation of SIFs along crack fronts and edges in three-dimensional problems has been presented in this paper. The proposed formulation has been implemented as a post-processing module in a BEM code, so it can be applied to a BEM solution at a later stage. The implementation takes advantage of the possibility given by the boundary integral representations to obtain directly only the required displacement and stress values at internal domain points. The present computational procedure is valid for finding SIFs $K_{mp}(z)$ (see expression (1)) associated to the leading (singular) term as well as other higher-order terms in the eigenfunction expansion which verify the condition $0 < \lambda_{mp} < \lambda_{\text{sing.}} + 1$, $\lambda_{\text{sing.}}$ representing the lowest singularity exponent in the asymptotic series expansion of the elastic solution at the edge neighbourhood.

The developed numerical tool has been employed to analyse two problems, one including a crack and the other a reentrant edge, in order to verify its capacity to capture a three-dimensional behaviour of SIFs. To assess the accuracy of the procedure developed, a 3-D crack configuration with known quadratic variation of $K_I(z)$ has been solved. An excellent agreement has been found between the analytic and computed results. In the second problem, a thick plate with a 270° dihedral solid angle has been modeled to study the variation of the $K_I(z)$ along the edge. The computed SIF presents only a modest variation in the vicinity of the middle of the specimen. In contrast, for the region near to the free lateral surface a boundary layer effect, characterized by a steep decrease, can be observed in $K_I(z)$ behaviour. The boundary layer effect has been studied for various Poisson's ratio v, finding that it is a function of v and that $K_I(z)$ has an asymptotic power law behaviour.

It should be stressed that accurate values of SIFs have been obtained using the present method without using either special singular elements or very fine meshes at the edge. Thus, first, no special requirements are imposed on BEM code (application of standard boundary elements is sufficient) and, second, computational resources and computing time required to obtain accurate results are significantly reduced.

Finally, note, that the present method to calculate $K_{mp}(z)$ can be easily extended to the case of 3-D multimaterial wedges, which will be presented in a forthcoming paper.

Acknowledgement

The present work has been carried out during the research stay of J.E.O. at the University of Seville funded by the Spanish Ministry of Education, Culture and Sport (Grant No. SB2002-201). V.M. and F.P. also acknowledge the financial support from the Spanish Ministry of Science and Technology (Project No. MAT2003-03315).

Appendix A. The three-dimensional crack solution

Consider an infinite elastic medium with a traction-free crack occupying the half plane defined by $y = 0$ and $x < 0$. The crack front coincides with the z-axis. Then the following expansion represents a linear elastic solution of a crack problem with $K_I(z)$ varying quadratically with z:

$$
\begin{aligned}
u_r &= \frac{9k\sqrt{r}z^2}{G}\left[(2\kappa-1)\cos\left(\frac{\theta}{2}\right)-\cos\left(\frac{3\theta}{2}\right)\right]-\frac{kr^{5/2}}{G}\left[3(2\kappa-5)\cos\left(\frac{\theta}{2}\right)+\frac{(b-c)}{5}\cos\left(\frac{3\theta}{2}\right)\right]\\
u_\theta &= \frac{9k\sqrt{r}z^2}{G}\left[\sin\left(\frac{3\theta}{2}\right)-(2\kappa+1)\sin\left(\frac{\theta}{2}\right)\right]+\frac{kr^{5/2}}{G}\left[\frac{(b+c-12)}{5}\sin\left(\frac{3\theta}{2}\right)+3(2\kappa+1)\sin\left(\frac{\theta}{2}\right)\right] \qquad \text{(A.1)}\\
u_z &= \frac{-12zr^{3/2}}{G}\left[3\cos\left(\frac{\theta}{2}\right)-(2\kappa+1)\cos\left(\frac{3\theta}{2}\right)\right]
\end{aligned}
$$

$$
\begin{aligned}
\sigma_{rr} &= \frac{9kz^2}{\sqrt{r}}\left[5\cos\left(\frac{\theta}{2}\right) - \cos\left(\frac{3\theta}{2}\right)\right] - kr^{3/2}\left[3a\cos\left(\frac{\theta}{2}\right) + b\cos\left(\frac{3\theta}{2}\right)\right] \\
\sigma_{\theta\theta} &= \frac{9kz^2}{\sqrt{r}}\left[3\cos\left(\frac{\theta}{2}\right) + \cos\left(\frac{3\theta}{2}\right)\right] + akr^{3/2}\left[3\cos\left(\frac{\theta}{2}\right) + \cos\left(\frac{3\theta}{2}\right)\right] \\
\sigma_{zz} &= \frac{72kvz^2}{\sqrt{r}}\cos\left(\frac{\theta}{2}\right) - 8kr^{3/2}\left[9\kappa'\cos\left(\frac{\theta}{2}\right) - (2\kappa+1)(2\kappa'+1)\cos\left(\frac{3\theta}{2}\right)\right] \\
\sigma_{r\theta} &= \frac{9kz^2}{\sqrt{r}}\left[\sin\left(\frac{\theta}{2}\right) + \sin\left(\frac{3\theta}{2}\right)\right] + 3k(a+6)r^{3/2}\left[\sin\left(\frac{\theta}{2}\right) + \sin\left(\frac{3\theta}{2}\right)\right] \\
\sigma_{\theta z} &= -36k\kappa z\sqrt{r}\left[\sin\left(\frac{\theta}{2}\right) + \sin\left(\frac{3\theta}{2}\right)\right] \\
\sigma_{rz} &= 36kz\sqrt{r}\left[(\kappa-2)\cos\left(\frac{\theta}{2}\right) + \kappa\cos\left(\frac{3\theta}{2}\right)\right]
\end{aligned}
\tag{A.2}
$$

where $a = 4\kappa - 7$, $b = 20\kappa + 1$, $c = 4(2\kappa+1)(\kappa-3)$, $\kappa = 3 - 4v$ and $\kappa' = 1 + v$, v being the Poisson ratio.

References

Andersson, B., Falk, U., Babuška, I., Petersdorff, T.B., 1995. Reliable stress and fracture mechanics analysis of complex components using a *h-p* version of FEM. International Journal for Numerical Methods in Engineering 38, 2135–2163.

Aksentian, O.K., 1967. Singularities of the stress–strain state of a plate in the neighbourhood of an edge. Journal of Applied Mathematics and Mechanics 31, 193–202.

Barsoum, R.S., 1976. On the use of isoparametric finite element in linear fracture mechanics. International Journal for Numerical Methods in Engineering 10, 25–37.

Bažant, Z.P., Estenssoro, L.F., 1979. Surface singularity and crack propagation. International Journal of Solids and Structures 15, 405–426.

Benthem, J.P., 1977. State of stress at the vertex of a quarter-infinite crack in a half-space. International Journal of Solids and Structures 13, 479–492.

Bueckner, H.F., 1973. In: Sih, G.C. (Ed.), Mechanics of Fracture: Methods of Analysis and Solution of Crack Problems. Noordhoff, Leyden, pp. 239–314.

Carpenter, W.C., 1984. Mode I and mode II intensities for plates with cracks of finite opening. International Journal of Fracture 26, 201–214.

Carpenter, W.C., 1995. Insensitivity of the reciprocal work contour integral method to higher order eigenvector. International Journal of Fracture 73, 93–108.

Chan, S.K., Tuba, I.S., Wilson, W.K., 1970. On the finite element method in linear fracture mechanics. Engineering Fracture Mechanics 2 (1), 1–17.

Chen, F.H.K., Shield, R.T., 1977. Conservation laws in elasticity of the *J*-integral type. Zeitschrift für Angewandte Mathematik und Physik (ZAMP) 28, 1–22.

Chen, G., Zhou, J., 1992. Boundary Element Methods. Academic Press Limited, Cambridge, Great Britain.

Choi, N.Y., Earmme, Y.Y., 1992. Evaluation of stress intensity factors in a circular arc-shaped interfacial crack using *L*-integral. Mechanics of Materials 14, 141–153.

Cisilino, A.P., Ortiz, J.E., 2005. Boundary element analysis of three-dimensional mixed-mode cracks via the interaction integral. Computer Methods in Applied Mechanics and Engineering 194, 935–956.

Costabel, M., Dauge, M., Yosibash, Z., 2004. A quasi-dual function method for extracting edge stress intensity functions. Society for Industrial and Applied Mathematics 35, 1177–1202.

Dunn, M.L., Hui, C.Y., Labossiere, P.E.W., Lin, Y.Y., 2001. Small scale geometric and material features at geometric discontinuities and their role in fracture analysis. International Journal of Fracture 110, 101–121.

Eshelby, R.D., 1956. The continuum theory of lattice defects. In: Seitz, F., Turnbull, D. (Eds.), Solids State Physics, vol. III. Academic Press.

Golub, G.H., Van Loan, C.F., 1989. Matrix Computation. The Johns Hopkins University Press, United States of America.

Hartranft, R.J., Sih, G.C., 1969. The use of eigenfunction expansions in the general solutions of three-dimensional crack problems. Journal of Mathematics and Mechanics 19 (2), 123–138.

Helsing, J., Jonsson, A., 2002. On the computation of stress fields on polygonal domains with V-notches. International Journal for Numerical Methods in Engineering 53, 433–453.

Henshell, R.D., Shaw, K.G., 1975. Crack tip finite elements are unnecessary. International Journal for Numerical Methods in Engineering 9, 495–507.

Huber, O., Nickel, J., Kuhn, G., 1993. On the decomposition of the *J*-integral for 3D crack problems. International Journal of Fracture 64, 339–348.

Im, S., Kim, K.S., 2000. An application of two-state *M*-integral for computing the intensity of the singular near-tip field for a generic wedge. Journal of the Mechanics and Physics of Solids 48, 129–151.

Irwin, G., 1957. Analysis of stresses and strains near the end of a crack traversing a plate. Journal of Applied Mechanics, ASME 24, 361–364.

Knowles, J.K., Sternberg, E., 1978. On a class of conservation laws in a linearized and finite elastostatics. Archive for Rational Mechanics and Analysis 44, 187–211.

Kwon, S.W., Sun, C.T., 2000. Characteristics of three-dimensional stress fields in plates with a through-the-thickness crack. International Journal of Fracture 104, 291–315.

Lachat, J.C., Watson, J.O., 1976. Effective numerical treatment of boundary integral equations: a formulation for three-dimensional elastostatics. International Journal for Numerical Methods in Engineering 10, 991–1005.

Lee, Y., Im, S., 2003. On the computation of the near-tip stress intensities for three-dimensional wedges via two-state *M*-integral. Journal of the Mechanics and Physics of Solids 51, 825–850.

Leguillon, D., 1995. Computation of 3D-singularities in elasticity. In: Costabel, M., Dauge, M., Nicaise, S. (Eds.), Boundary Value Problems and Integral Equations in Nonsmooth Domains, pp. 161–170.

Leguillon, D., Sanchez-Palencia, E., 1987. Computation of Singular Solutions in Elliptic Problems and Elasticity. Masson–John Wiley, Paris–New York.

Leguillon, D., Sanchez-Palencia, E., 1999. On 3D cracks intersecting a free surface in laminated composites. International Journal of Fracture 99, 25–40.

Li, F.Z., Shih, C.F., Needleman, A., 1985. A comparison of methods for calculating energy release rates. Engineering Fracture Mechanics 21 (2), 405–421.

Meda, G., Messmer, T.W., Sinclair, G.B., Solecki, J.S., 1998. Path-independent *H* integral for three-dimensional fracture mechanics. International Journal of Fracture 94, 217–234.

Miyazaki, N., Ikeda, T., Soda, T., Munakata, T., 1993. Stress intensity factor analysis of interface crack using boundary element method—application of contour-integral method. Engineering Fracture Mechanics 45, 599–610.

Nakamura, T., Parks, D.M., 1988. Three-dimensional stress field near the crack front of a thin elastic plate. Journal of Applied Mechanics 55, 805–813.

Ortiz, J.E., Cisilino, A.P., 2005. Three-dimensional boundary element assessment of a fibre/matrix interface crack under transverse loading. Computers and Structures 83, 856–869.

Paegau, S.S., Gadi, K.S., Biggers, S.B., Joseph, P.F., 1996. Standardized complex and logarithmic eigensolutions for *n*-material wedges and junctions. International Journal of Fracture 77, 51–76.

Rice, J.R., 1968. A path independent integral and the approximate analysis of strain concentration by notches and cracks. ASME Journal of Applied Mechanics 35, 379–386.

Rigby, R.H., Aliabadi, M.H., 1993. Mixed-mode *J*-integral method for analysis of 3D fracture problems using BEM. Engineering Analysis with Boundary Elements 11, 239–256.

Savruk, M.P., Shakarayev, S.V., 2001. Stress singularities for three-dimensional corners using the boundary integral equation method. Theoretical and Applied Fracture Mechanics 36, 263–275.

Seweryn, A., 1994. Brittle fracture criterion for structures with sharp notches. Engineering Fracture Mechanics 47, 673–681.

Seweryn, A., 1996. Elastic stress singularities and corresponding generalized stress intensity factor for angular corners under various boundary conditions. Engineering Fracture Mechanics 55, 529–556.

Shih, C.F., Moran, B., Nakamura, T., 1986. Energy release rate along a three-dimensional crack front in a thermally stressed body. International Journal of Fracture 30, 79–102.

Sinclair, G.B., 1979. Asymptotic singular eigenfunctions for the three-dimensional crack. In: Proceedings of the Seventh Canadian Congress of Applied Mechanics, Sherbrooke, Quebec, pp. 295–296.

Sinclair, G.B., Okajima, M., Griffin, J.H., 1984. Path independent integrals for computing stress intensity factors at sharp notches in elastic plates. International Journal for Numerical Methods in Engineering 20, 999–1008.

Sládek, V., Sládek, J., 1986. Improved computation of stresses using the boundary element method. Applied Mathematic Modelling 10, 249–255.

Szabó, B.A., Babuška, I., 1991. Finite Element Analysis. John Wiley & Sons, New York.

Vasilopoulos, D., 1988. On the determination of higher order terms of singular elastic stress fields near corners. Numerische Mathematik 53, 51–95.

Wieghardt, K., 1907. Über das Spalten und Zerreissen elastischer Körper. Zeitschrift für Mathematik und Physik 55, 60–103 (English translation by H.P. Rossmanith, Fatigue and Fracture of Engineering Materials and Structures 18, 1371–1405, 1995).

Williams, M.L., 1952. Stress singularities resulting from boundary conditions in angular corners of plates in extension. Journal Applied Mechanics 19, 526–528.

Williams, M.L., 1957. On the stress distribution at the base of a stationary crack. Journal of Applied Mechanics 24, 109–114.

Wolfram, S., 1991. Mathematica, A System for Doing Mathematics by Computer. Addison-Wesley, Redwood City.

Yosibash, Z., Bussiba, A., Gilad, I., 2004. Failure criteria for brittle elastic materials. International Journal of Fracture 125, 307–333.